# Homology modeling and deletion mutants of human nicotinamide mononucleotide adenylyltransferase isozyme 2: New insights on structure and function relationship

**Lucia Brunetti,[†] Michele Di Stefano,[†] Silverio Ruggieri, Flavio Cimadamore,* and Giulio Magni***

Dipartimento di Patologia Molecolare e Terapie Innovative, sezione di Biochimica, Università Politecnica delle Marche, 60131 Ancona, Italy

Received 22 June 2010; Revised 30 August 2010; Accepted 4 October 2010
DOI: 10.1002/pro.526
Published online 15 October 2010 proteinscience.org

**Abstract: Nicotinamide mononucleotide adenylyltransferase (NMNAT) catalyzes the formation of NAD by means of nucleophilic attack by 5′-phosphoryl of NMN on the α-phosphoryl group of ATP. Humans possess three NMNAT isozymes (NMNAT1, NMNAT2, and NMNAT3) that differ in size and sequence, gene expression pattern, subcellular localization, oligomeric state and catalytic properties. Of these, NMNAT2, the least abundant isozyme, is the only one whose much-needed crystal structure has not been solved as yet. To fill this gap, we used the crystal structures of human NMNAT1 and NMNAT3 as templates for homology-based structural modeling of NMNAT2, and the resulting raw structure was then refined by molecular dynamics simulations in a water box to obtain a model of the final folded structure. We investigated the importance of NMNAT2's central domain, which we postulated to be dispensable for catalytic activity, instead representing an isozyme-specific control domain within the overall architecture of NMNAT2. Indeed, we experimentally confirmed that removal of different-length fragments from this central domain did not compromise the enzyme's catalytic activity or the overall tridimensional structure of the active site.**

**Keywords: homology modeling; NMNAT; protein domain; deletion mutants**

## Introduction

While NAD is an essential and ubiquitous coenzyme that plays fundamental roles in cellular redox reactions, its cleavage is essential for such protein modification reactions as histone deacetylation by the sirtuins[1–3] and mono- and poly-(ADP-ribosyl)ation by ARTs and PARPs, respectively.[4–7] NAD also participates in calcium ion signaling through its derivative nicotinic acid adenine dinucleotide phosphate (NaADP) and degradation products ADP-ribose and cyclic ADP-ribose.[8] What is now abundantly clear is that NAD homeostasis (i.e., synthesis, transformations, and degradation) is of utmost significance in cellular energy metabolism, signal transduction and chromatin stability and remodeling.

During the preparation of this manuscript, a report by Lau C. et al. confirming the full dispensability of the NMNAT2 central domain for the catalytic activity and the importance of the cysteine 164–165 residues for the golgian localization appeared in the literature (Lau C, Dolle C, Gossmann TI, Agledal L, Niere M, Ziegler M (2010) Isoform-specific targeting and interaction domains in human nicotinamide mononucleotide adenylyltransferases. J Biol Chem 285:18868–18876).

[†]Brunetti L. and Di Stefano M. contributed equally to this work.

**Correspondence to:* Flavio Cimadamore, Burnham Institute for Medical Research, 10901 North Torrey Pines Road, La Jolla, CA 92037. E-mail: flavioc@burnham.org (or) Giulio Magni, Dipartimento di Patologia Molecolare e Terapie Innovative, sezione di Biochimica, Università Politecnica delle Marche, via Ranieri 69, 60131 Ancona, Italy. E-mail: g.magni@univpm.it

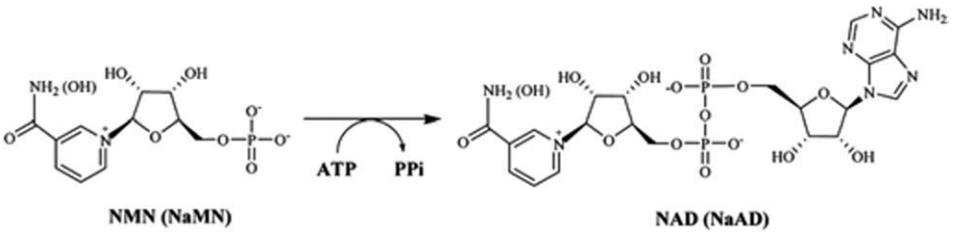


**Figure 1.** The NMNAT catalyzed reaction. NMN: nicotinamide mononucleotide; NaMN: nicotinic acid mononucleotide; NAD: nicotinamide adenine dinucleotide; NaAD: nicotinic acid adenine dinucleotide.

Nicotinamide mononucleotide adenylyltransferase (NMNAT, EC 2.7.7.1) is the central enzyme of the NAD biosynthesis, catalyzing the transfer of the adenylyl moiety of ATP to NMN (or to its deamidated form NaMN)[9–14] (Fig. 1).

In humans, three different NMNAT isozymes have been identified and extensively characterized both at the molecular and biochemical levels. They differ in size, kinetic properties, tissue expression, subcellular compartmentation and oligomeric state.[15]

The structure of human NMNAT1 (hNMNAT1), a 279-residue nuclear protein expressed in all tissues, has been independently solved in three different laboratories and determined in the absence and presence of its substrates and products.[16–18]

Human NMNAT2 (hNMNAT2), a 307-residues enzyme that shares 34% sequence identity with NMNAT1, is uniquely localized within the Golgi complex.[15] Unlike NMNAT1 and NMNAT3 which are oligomeric, gel filtration studies indicate that NMNAT2 is monomeric.[19] Concerning its distribution in human tissues, the protein is most abundant in brain, but is also present in heart and skeletal muscle.[19,20]

The tissue-specific expression pattern of human NMNAT3 (hNMNAT3), a 252-residues mitochondrion localized protein, differs from NMNAT1. In particular, NMNAT3 is present in lung, spleen,[15] red blood cells,[21] and, to a lesser extent, in placenta and kidney.[22] The 3D structure of NMNAT3 has been solved in its ligand-free form and when complexed to NMN, NAD, NaAD and an ATP analogue.[22]

Overall these data suggest that these isozymes have specific and distinctive roles, rather than being merely redundant in their function.

The relevance of human NMNAT isozymes is underscored by their involvement in several pathways of the cellular metabolism.

In particular, NMNAT is a target of emerging importance in cancer chemotherapy, chiefly because most tumoral tissues reveal low NMNAT expression with respect to normal tissues[23] and because treatment with isozyme-specific NMNAT inhibitors promises to reduce NMNAT activity, thereby deplete NAD below that needed for cancer cell survival. In addition, NMNAT is responsible for the metabolic activation of the antineoplastic compounds of the tiazofurin class: these compounds are intracellularly converted by nucleoside kinase and NMNAT in their corresponding NAD analogues, such that their antineoplastic action is related to their ability to inhibit IMP dehydrogenase, ultimately blocking purine biosynthesis.[24,25]

NMNAT has also been involved in the protection against neurodegenerative disorders, being able to slow the Wallerian degeneration in mutant mice, that is, axonal self-destruction in response to axonal injury.[26–28] Recent works demonstrated the involvement of NMNAT2 in this process,[29,30] even though its neuroprotective effects are still debated. Finally, NMNAT is also recognized as a promising target for the development of novel antibacterial drugs,[31] mainly because NAD is essential for microbial cell survival and because there are significant differences in the active site structures of bacterial and the human NMNATs.

Such considerations demand the comparative analysis of human and bacterial NMNAT structures, an enterprise that should enable the design of selective NMNAT inhibitors with high potential as modulators of human NAD metabolism and as antibiotics.

While NMNAT1 and NMNAT3 and several bacterial NMNATs have been structurally characterized,[32] NMNAT2 has resisted 3D structural analysis, owing its poor solubility and its susceptibility to aggregation (unpublished results). In such situations, our computational approach represents a powerful tool to fill voids in the understanding of its distinctive structural properties.

In this report, we now provide a homology-based model of human NMNAT2 that uses published structures of human NMNAT1[17] and NMNAT3[22] as templates, followed by refinement with molecular dynamics simulations in a "water box". The results of the simulation and the comparison with the other human isozymes prompted us to make some interesting considerations on NMNAT2 structure-function relationship.

In addition to analyzing the NMNAT2 structure *in silico*, we also investigated the relevance of the enzyme's central region, which shows no sequence homology with NMNAT1 or NMNAT3 (Fig. 2). This central region represents a distinct structural unit in the overall predicted architecture of NMNAT2,


**Figure 2.** Multiple alignment of the three human NMNAT isozymes.

and we generated and functionally characterized NMNAT2 mutants whose central region was lacking variable-length aminoacid stretches. Our findings demonstrate that this region is not directly involved in enzyme catalysis.

## Results

### *Homology modeling*

Our model obtained for NMNAT2 structure prediction (Fig. 3) includes residues 5-303, because the first four residues correspond to the disordered N-terminus of the already solved NMNAT1 and NMNAT3 structures.[16–18,22]

A Ramachandran plot for the refined structure (Fig. 4) was evaluated using the program PROCHECK[33]: 232 residues were in the most favored regions, 29 residues were in the additional allowed regions, one residue (Q300) in a generously allowed region and only two residues (D286 and Y302) in the disallowed region. Overall, 98.9% of the nonglycine and nonproline residues were in the most allowed or in the additional allowed regions highlighting the good geometry of the model.

Superimposition of the NMNAT2 model with the NMNAT1 and NMNAT3 template structures yielded backbone root mean square deviation (RMSD) values (e.g., 2.35 Å for 1KQN, 2.39 Å for 1NUU, 2.40 Å for 1KQO, and 2.40 Å for 1NUQ) for the most conserved regions that are in agreement with a good modeling of the conserved core.

The reported three-dimensional structures for NMNAT1 and NMNAT3 present an unresolved central region,[16–18,22] and NMNAT2's central region (residues 103–196; See Fig. 2) shows no homology with the corresponding sequences of the NMNAT1 and NMNAT3 isozymes or, for the matter, with any other proteins in the PDB database. Therefore, this region was folded by using a template based on a library of short peptides of known X-ray structure, as automatically returned from the SWISS-MODEL server.[34] We identified five putative helices (represented by residues 106–113, 117–123, 135–152, 158–174, 183–193), linked by several loops.

To evaluate our model, we considered its stability during the simulation by measuring the RMSD of the C-α as a function of time over the entire 500 ps simulation. We computed separately the RMSD both for the region 106–193 of the NMNAT2 model and for a model lacking this region and representing the conserved region (Fig. 5). It can be noted that the last model showed great stability for the whole simulation with an RMSD plateau of ~0.18 nm, while the region 106–193 showed a progressive drift with a major RMSD plateau of ~0.3 nm. To examine the structural fluctuation on a residue by residue basis, we computed the time-averaged root mean square fluctuation (RMSF) of the C-α for the whole

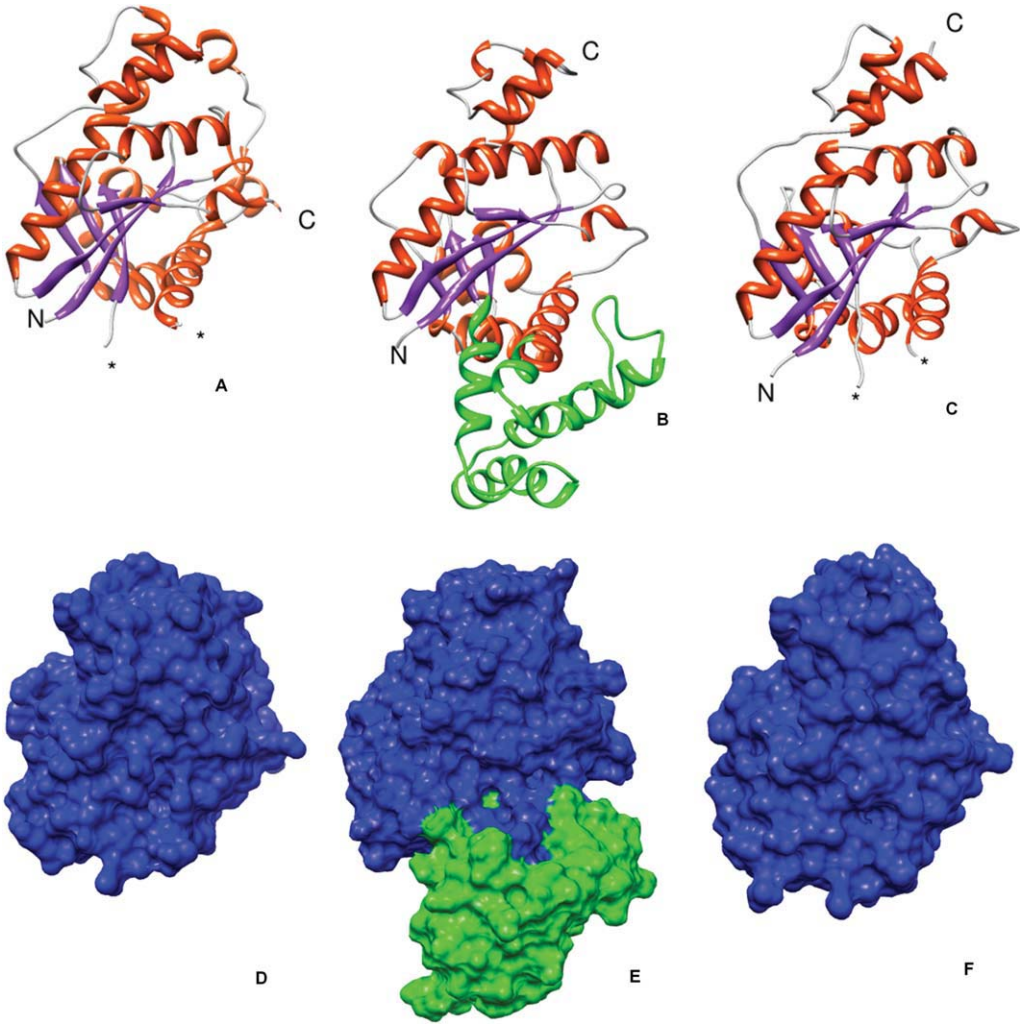


**Figure 3.** Structural representation of the three NMNAT isozymes. Ribbon diagram of NMNAT1 (PDB code 1KQN) (A), our predicted NMNAT2 model (B), and NMNAT3 (PDB code 1NUP) (C) with their respective molecular surfaces (D,E,F). N and C indicate the amino- and carboxy- termini of the polypeptide chain, respectively. The positions of the disordered central regions on NMNAT1 and 3, missing in the PDB structure files, are indicated with asterisks (*), whereas the putative disordered corresponding region of NMNAT2 is represented both in ribbon and surface visualization (B and E). [Color figure can be viewed in the online issue, which is available at wileyonlinelibrary.com.]

model (Fig. 6). Also in this case, the N- and C-termini were very stable, while the central region underwent the major displacement.

The stability of NMNAT2 Δ106–193 was further suggested by the calculation of the distances between the centers of mass of the N- and C-terminal domains and the number of hydrogen bonds formed between them as a function of time [Fig. 7(A,C)]. Both parameters were very stable during the simulation, and a mean of 11.83 ± 1.86 hydrogen bonds appeared to stabilize the interaction between the two domains, with their mass centers showing a mean distance of 1.11 ± 0.02 nm. Similar calculations were performed between the central and the N- and C-terminal regions.

The results, reported in Figure 7(B,D), show a slight progressive decrease of the distance between these regions, possibly due to a simple random drift of the central one or to a progressive interaction between them. In the latter hypothesis, since the number of formed hydrogen bonds appears to be quite constant during the simulation (9.47 ± 1.68), the progressive interaction could well be attributable to hydrophobic forces.

To visualize the detailed interactions of the docked poses of the natural ligands, the AUTODOCK 4.0.2[35] program was used. Docking studies with NMN, ATP and NAD concerned the NMNAT2 three-dimensional model obtained through homology modeling. The residues involved in recognition and stabilizing interactions of natural ligands were the same indicated for NMNAT1[17,18] and NMNAT3[22] (unpublished results).

### *NMNAT2 deletion mutants*

To investigate the importance of the central domain of NMNAT2 on the catalytic properties of the

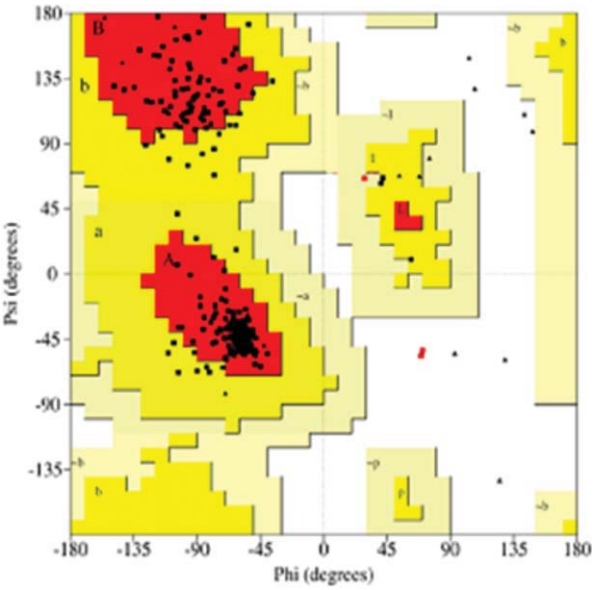


**Figure 4.** Ramachandran plot of NMNAT2 predicted model. [Color figure can be viewed in the online issue, which is available at wileyonlinelibrary.com.]

protein, we generated four mutants lacking amino acid stretches of different length in the domain. With respect to wild type NMNAT2, the deletion mutants lacked residues I113-R194 (mutant Δ82), I126-R194 (mutant Δ69), I152-R194 (mutant Δ43), and I163-R194 (mutant Δ32) (Fig. 2).

Upstream to the different deletions, the mutagenesis resulted in the substitution of C112 with W in Δ82 mutant, V125 with G in Δ69 mutant, and K151 with R in Δ43 mutant.

All mutants were over-expressed in *E. coli* BL21 cells showing expression levels comparable to that showed by the wt protein (Fig. 8).

The resulting recombinant proteins were purified by affinity chromatography on a nickel-based Ni-NTA resin (Fig. 9), and their NMNAT activities were determined spectrophotometrically. The results of such activity measurements demonstrated catalytic activities that were comparable, if not slightly

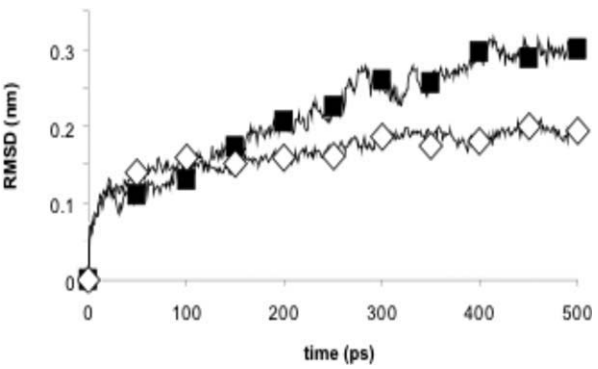


**Figure 5.** RMSD of the C-alpha of the NMNAT2 model. ◇:NMNAT2Δ(106–193); ■:region 106–193. See text for explanation.

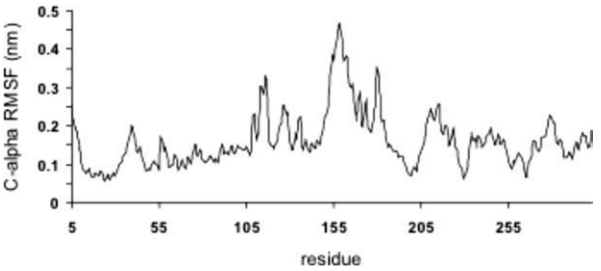


**Figure 6.** RMSF of the C-alpha of the NMNAT2 model.

higher, than that of the wt protein. In particular wt NMNAT2 showed a specific activity of 4.42 U/mg, whereas Δ82, Δ69, Δ43, and Δ32 showed specific activities of 6.83 U/mg, 6.62 U/mg, 7.22 U/mg, and 6.95 U/mg, respectively.

To investigate the influence of the central domain on the NMNAT2 sensitivity to magnesium ions, the purified recombinant proteins were subjected to our highly reliable HPLC-based NMNAT assay in the presence of various concentration of $MgCl_2$, ranging from 0 to 20 mM. All deletion mutants showed a behavior comparable to that exhibited by the wt protein. In particular, at 20 or 50 μM $MgCl_2$, all proteins exhibited about 20 or 45% of activity, respectively, with respect to the activity at 20 mM $MgCl_2$ (100%).

Finally, the purified mutants were subjected to gel filtration experiments to determine their oligomerization state. All proteins showed a native molecular mass in the range 30–40 kDa, as expected for the mass of the monomeric form of the mutated proteins.

## Discussion

Because NMNAT is widely regarded as an important druggable target for chronic and infectious diseases, there is a remarkable interest in gaining structural insights for guiding the development of high-affinity NMNAT inhibitors.[36]

Rational drug design of NMNAT inhibitors requires a detailed knowledge of the enzyme 3D structure, focusing on the distinct features of human NMNAT isozymes, which are also known to differ with respect to their tissue expression, state of oligomerization, subcellular localization, and certain catalytic properties.[15] Inasmuch as NMNAT2 is the only human NMNAT for which there is no solved three-dimensional structure yet, this study focused on obtaining a homology model of this protein, based on NMNAT1 and NMNAT3 crystal structures.[17,22]

Amino acid sequences alignment between the three human NMNATs shows a high degree of sequence homology spanning the N- and C-terminal regions, which likewise contain certain signatures common to all NMNATs (e.g., GXXXPX(T/H)XXH at the amino-terminal and SX(T/S)XXR at the carboxy-

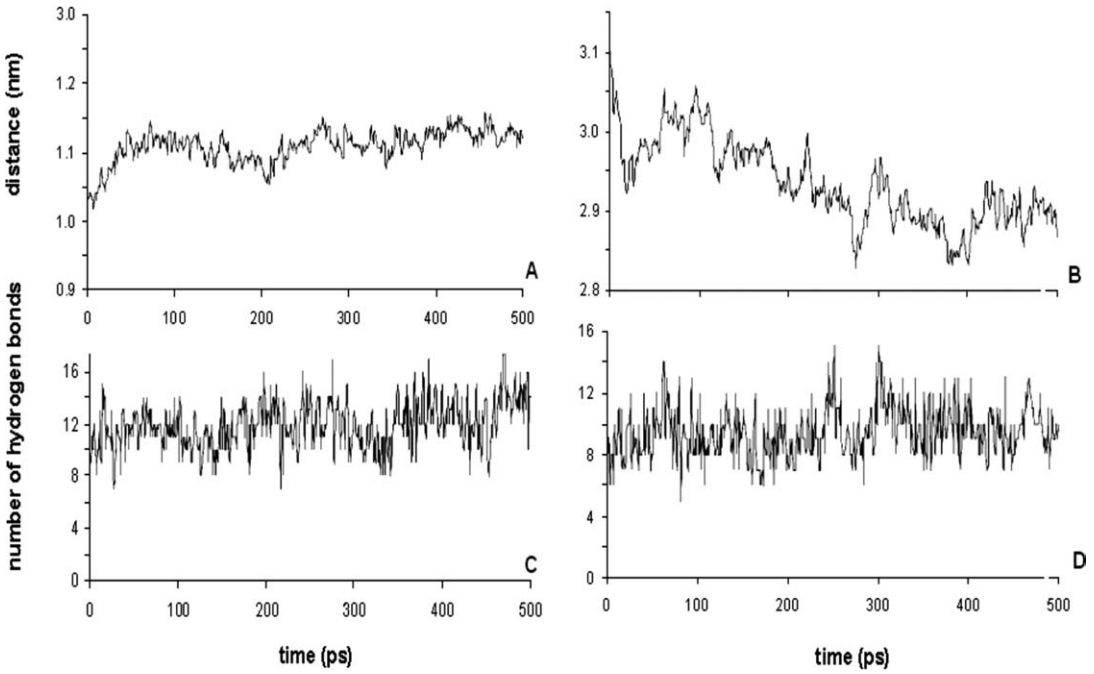


**Figure 7.** Distances between the centers of mass of the N- and C-terminal conserved domains (A) and between the global conserved domain and the central region 106–193 (B). Number of hydrogen bonds between the N- and C-terminal domains (C) and between the global conserved domain and the central region 106–193 (D). Angle and length cut-off for H-bonds detection are 60° and 2.5 Å, respectively.

terminal) and are linked by an extremely variable central region that is not conserved both in chain length and sequence. The only features common to NMNAT1 and NMNAT3 central regions are the disordered state and the high flexibility. In fact, the crystallographic studies carried out to date on these two proteins have been unable to assign a tertiary structure to these regions, whose coordinates are therefore missing in the structures deposited in the Protein Data Bank.[16–18,22]

The overall architecture of the conserved N- and C-terminal domains consists of a classical Rossmann fold[37] (six β-sheets surrounded by several α-helices) typical of nucleotide-binding proteins. In Figure 3 a comparison between the refined NMNAT2 model with crystallographic NMNAT1 and NMNAT3 structures is reported. The secondary structure analysis of the predicted model reveals that the N-terminal domain is composed by three β-sheets and four helices, while the C-terminal contains three β-sheets and seven helices. These two domains bend toward

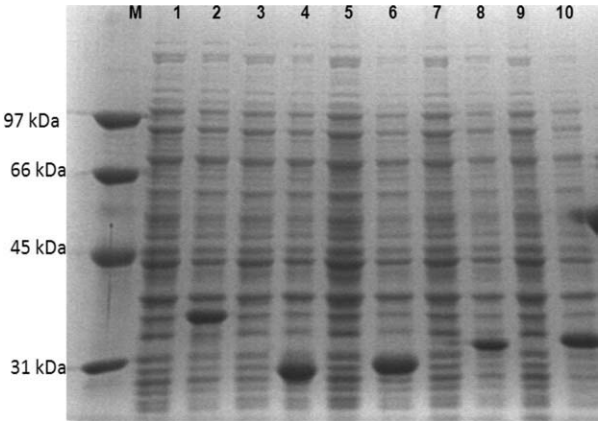


**Figure 8.** SDS-PAGE (10% polyacrilamide gel) of BL21 cells hyper-producing wt and deletion mutants NMNAT2: *M* = molecular weight standard; Lanes 1, 3, 5, 7, 9: BL21 cells hyper-producing wtNMNAT2, Δ82, Δ69, Δ43, and Δ32, respectively, before induction; lanes 2, 4, 6, 8, 10: BL21 cells hyperproducing wtNMNAT2, Δ82, Δ69, Δ43, and Δ32, respectively, after induction.

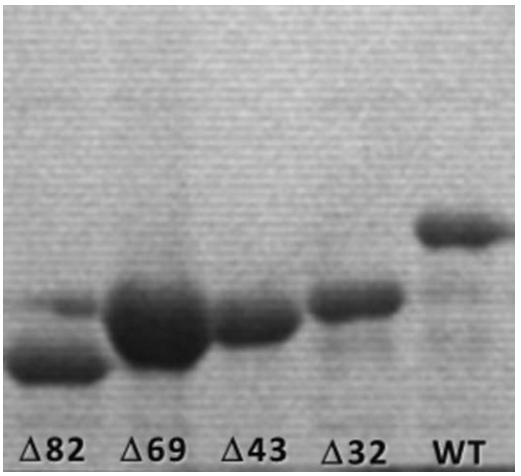


**Figure 9.** Tricine SDS-PAGE (10% polyacrilamide gel) of purified recombinant proteins. The different band migration corresponding to the different protein sizes can be observed.

the central region to reconstruct the Rossmann fold represented by a strongly twisted six-stranded parallel β-sheet core surrounded by the helices. The central domain, taken as automatically returned from the SWISS-MODEL server, is composed by five helices linked by several loops, with the first helix modeled as a continuation of the last helix of the N-terminal domain.

The overall model is particularly reliable at the level of the conserved N- and C-terminal domains, which represent the catalytic core and which have shown a high stability during the simulation. The central domain instead shows a slightly higher instability and mobility and, considering the analogy with the corresponding central disordered regions of NMNAT1 and NMNAT3, could be a flexible disordered region too. As a further support to this speculation, we found that the DisEMBL[38] server (http://dis.embl.de/) predicts a disordered state for this region.

In light of its reliability, the predicted NMNAT2 model has been used for docking studies that were performed to validate the putative active site localization. As expected, the results showed that the active site was localized at the level of the conserved N- and C-terminal regions and the residues involved in enzyme-substrates/product interactions were the same conserved residues reported for NMNAT1[17,18] and NMNAT3.[22] None of the residues of the central region was involved in stabilizing interactions; indeed this region appeared to stick out of the remaining catalytic core (Fig. 3).

To further analyze this aspect, we investigated the requirement of the central domain on the catalytic activity of the protein.

We presume that the nonconserved NMNAT central region has noncatalytic functions, perhaps required for subcellular localization, interaction with other proteins or even controlling enzyme turnover. For example, in the NMNAT1 primary structure both the nuclear localization signal[39] $^{123}$PGRKRKW$^{129}$ and S136, representing the phosphorylation site involved in the modulation of the interaction with PARP1,[40] are included in the central domain. Likewise the central domain of NMNAT2 is probably responsible for localizing this isozyme to the Golgi apparatus; interestingly the central domain contains the two adjacent C164 and C165, a distinctive structural element among NMNAT family members.[32,41] On the other hand, the mitochondrial localization of NMNAT3 presumably depends on its predicted N-terminal mitochondria-targeting sequence.[42]

In light of the solved NMNAT1 and NMNAT3 3D structures and our energy-minimized homology-NMNAT2 model, we suggest that these central domains represent distinctive structural noncatalytic units.

We thus investigated the influence of the isozyme-specific central domain of NMNAT2 on the enzymatic activity/protein fold, by generating NMNAT2 mutants lacking different-length stretches within this domain. The smallest deletion removed 32 residues, whereas the more extended deletion removed a total of 82 residues, corresponding to nearly the entire domain.

All deletion mutants retained the ability to catalyze NAD synthesis from NMN and ATP, demonstrating that the central domain is not essential for functional folding of the catalytic core. Notably, the deletion mutants had higher specific activities than observed with wt enzyme. We speculate that they may fold in particular stabilized conformations that may activate catalysis, perhaps by increasing substrate accessibility to the catalytic core. In principle, such activity-enhancing conformations might be achieved *in vivo* through interaction of the central domain with other specific proteins or metabolic regulators.

Beyond analyzing the significance of NMNAT2's central domain for catalytic activity, we investigated its possible involvement in the functional and structural properties of the protein, that is, its sensitivity to magnesium ions and its oligomeric organization.

Among the three human isozymes, NMNAT2 is the most sensitive to magnesium ions concentration, exhibiting activity even at very low metal concentration.[43] To learn if the central domain could influence such catalytic ability, the purified recombinant mutants were assayed in the presence of various concentrations of $MgCl_2$. We found that the sensitivity of NMNAT2 to magnesium ions is independent on the central domain, because all deletion mutants and the wild type enzyme showed comparable activation by this divalent cation (data not shown).

Finally we investigated the importance of the central domain for the oligomerization state of the protein.

Gel filtration experiments showed that NMNAT2 exists as a monomeric protein in solution,[19] differently from NMNAT1 and NMNAT3 which exhibit an oligomeric organization.[16,22] Considering the high homology between the conserved globular structures solved for NMNAT1 and NMNAT3 and our predicted NMNAT2 model, it could be presumed that the monomeric state of NMNAT2 is determined by the presence of the central domain, which might hinder intermolecular interactions between different NMNAT2 monomers. Even so, the central-domain deletion mutants exhibited the same monomeric state as wt NMNAT2.

In summary, this report represents the first attempt to predict the 3D structure of human NMNAT2 by means of homology modeling. We found that the fold of NMNAT2 is virtually superimposable to those of NMNAT1 and NMNAT3, especially in the conserved N- and C-terminal regions, which form a globular catalytic unit characterized by a Rossmann fold. Our experimental results showed that the nonconserved central region is dispensable for the

enzymatic activity and, probably, for the 3-D folding of the catalytic core of the enzyme. This is in keeping with both the homology model, which shows the central domain as a sticked out structural unit, and the molecular docking simulations, which suggest that the residues interacting with substrates and NAD reside in the N- and C-terminal conserved regions.

## Materials and Methods

### Homology modeling

A raw structure of NMNAT2 was determined by means of homology modeling using SWISS-MODEL,[34,44,45] an automated protein modeling server. The model was based on both the alignment with amino acid sequences of NMNAT1 (31.8% identity with NMNAT2) and NMNAT3 (32.7% identity with NMNAT2) (Fig. 2) and their structures when complexed with the substrates NAD (PDB code 1KQN[17] for NMNAT1 and 1NUU for NMNAT3[22]) and NaAD (PDB code 1KQO for NMNAT1[17] and 1NUQ for NMNAT3[22]).

Amino acid sequence alignments were carried out with CLUSTAL-W[46–48] algorithm, followed by manual refinement using the SWISS-PDB viewer program.[34] The structural stability of the model returned from the server was tested by means of molecular dynamics simulation using the GROMACS simulation package[49,50] which solves the Newtonian equations of motion for the desired system, thereby calculating how atomic coordinates vary as a function of time.

The simulation was performed by using the SWISS-PDB viewer software in which the raw model obtained from the homology modeling was superimposed with the crystal structure of NMNAT1 in complex with NMN (PDB code: 1GZU[18]). The structure was energy-minimized *in vacuo* using 1000 steps of steepest descent to remove distorted geometries and it was embedded in a solvent box consisting of 9418 single point-charge water molecules[51] and a $Mg^{2+}$ ion added to remove the negative net charge of the system. The next step consisted of a canonical 20 ps simulation with position restraints to the protein (necessary for randomization of the water molecules surrounding the model) followed by a 500 ps unrestrained simulation. All the simulations were performed coupling the solvent, the cation and the protein separately to the thermal bath at 300 K (coupling constant = 0.1 ps) and applying an isotropic constant pressure of 1 bar (coupling constant = 0.5 ps, compressibility = 4.5 X 10-5 bar-1). Particle Mesh Ewald algorithm[52,53] was used to compute the electrostatic interactions. The protein, water, and ion parameters were those of the Gromacs force field. The last 80 ps of the 500 ps simulation were used to compute an average structure for the NMNAT2, which, after minimization with 1000 steps of steepest descent, represents our final model [Fig. 3(B)]. 3D rendering was done with VMD[54] or SWISSPBD viewer softwares.[34] Other analyses were performed using scripts included in the Gromacs package.

**Table I.** *Primers Used in This Study*

| | Sequence (5′-3′) |
|---|---|
| Δ82-FW | GAGGGTGACTGGCTGGATCCTCTCCAATGTC |
| Δ82-REV | GACATTGGAGAGGATCCAGCCAGTCACCCTC |
| Δ69-FW | CTTCCATGACACCTGGGATCCGACAGCCACA AAACG |
| Δ69-REV | CGTTTTGTGGCTGTCGGATCCCAGGTGTCA TGGAAG |
| Δ43-FW | GCCCACTGCAGCCAGGATCCTGGGGAAGG TGGGAG |
| Δ43-REV | CTCCCACCTTCCCCAGGATCCTGGCTGCA GTGGGC |
| Δ32-FW | AAAGCCTCAGCCGGATCCGCTGTGTCCGCCC |
| Δ32-REV | GGGCGGACACAGCGGATCCGGCTGAGGCTTT |
| 2-28c-FW | ATTTGACATATGACCGAGACCACCAAGAC |
| 2-28c-REV | ATTAAGCTTCTAGCCGGAGGCATTGATG |

### NMNAT2 deletion mutants

***NMNAT2 cloning.*** Human NMNAT2 open reading frame was amplified by PCR from pET15b-NMNAT2 recombinant vector.[19] Appropriate primers carrying *HindIII* and *NdeI* restriction overhangs for directional cloning into the polylinker region of pET28c (Novagen) were used (primers 2-28c-FW and 2-28c-REV, Table I). The resulting construct pET28c-NMNAT2 was replicated in *E. coli* TOP10F' strain (Invitrogen) and verified by sequencing before use in protein expression in *E. coli* BL21 strain.

***NMNAT2 central domain removal.*** A unique *BamHI* site is present in the NMNAT2 coding sequence (nucleotides 581–586). According to CLUSTAL-W multiple alignment of the three NMNAT isozymes (Fig. 2), the corresponding amino acids (R194–L196) are located at the end of the nonconserved central region of NMNAT2.

Four additional *BamHI* restriction sites were inserted by site-directed mutagenesis into the coding sequence of the central region by using the Quick change XL site-directed mutagenesis kit (Stratagene) and appropriate primers (Table I). The new *BamHI* sites were inserted in nucleotide positions 335–340 (corresponding to aminoacids C112–L114), 374–379 (V125–G127), 452–457 (K151–L153), and 485–490 (R162–C164). The plasmid template used for mutagenesis was the pET28c carrying the wt NMNAT2 gene.

The mutated plasmids were replicated in TOP10F' *E. coli* strain and cleaved by *BamHI*. After the removal of the cleaved fragments by loading on agarose gel, the resulting plasmids were purified,

religated by using T4 DNA Ligase, and replicated in TOP10F'. After sequencing validation, the plasmids were transformed in *E. coli* BL21 and used for the hyper-production of the mutated proteins.

***Protein expression and purification.*** Cultures of *E. coli* BL21 cells carrying pET28c plasmids encoding for wt NMNAT2 or its deletion mutants were grown in an incubator shaker (200 rpm) at 28°C in Luria-Bertani medium supplemented with 50 μg/mL kanamicin. When cultures reached an $OD_{600nm}$ of 0.6–0.8, induction was initiated by adding 1 mM IPTG followed by incubation for 4 h.

Induced cells were harvested by centrifugation (5000*g*, 10 min, 4°C) and resuspended in 1/20 vol of original culture with lysis buffer composed by 50 mM Na-phosphate (pH 7.5), 300 mM NaCl, 10 mM imidazole, and 5 mM CHAPSO, freshly supplemented with 1 mM TCEP, 1 mM PMSF, and 0.02 mg/mL leupeptine, antipain, chymostatin, pepstatin and aprotinin. Cells were lysed by sonication (20 s, 0.5 s intervals, 50 W). The crude extracts were clarified by centrifugation at 27,000*g* for 20 min at 4°C for subsequent protein purification. The His-tagged wt and deletion mutants NMNAT2 were purified by Ni-NTA (Qiagen) affinity chromatography. Briefly, the clarified supernatans were mixed with Ni-NTA resin (0.1 mL of resin per mL of crude extract) previously equilibrated with 50 mM Na-phosphate (pH 7.5), 300 mM NaCl, 10 mM imidazole, 1 mM TCEP, and left in gentle agitation at 4°C. After 30 min, the resin-containing crude extracts were loaded onto columns (6 cm × 1cm) and the flow-throughs were discarded. After washing with 25 mM imidazole in the same buffer, the elution of recombinant proteins was carried out by a single step increase of imidazole concentration to 250 mM. All purification steps were performed at 4°C. Chromatographic fractions were subjected to tricine SDS-PAGE[55] and tested for NMNAT activity by a spectrophotometric assay. Active and homogeneous fractions were pooled and stored at 4°C. Protein concentration was determined by the Bradford method,[56] using Bovine Serum Albumin (BSA) as the standard.

***NMNAT activity.*** NMNAT activity of wt and mutated NMNAT2 was measured by a spectrophotometric coupled assay or by an HPLC-based assay.[57]

Concerning the spectrophotometric assay, the standard reaction was performed at 37°C in a 1-mL, 1-cm-path cuvette, in final volume of 0.4 mL. The incubation mixture contained 172.5 μL ethanol reagent (1% V/V ethanol, 70 mM Tris-HCl pH 7.5, 8.4 mg/mL semicarbazide/HCl), 11.25 μg Alcohol dehydrogenase (ADH, 4 units), 225 μg BSA, 25 mM $MgCl_2$, 1 mM ATP, 1 mM NMN and the appropriate amount of purified NMNAT2. The reaction was usually started by the addition of NMN. The increase in absorbance was recorded continuously at 340 nm and from the slope of the linear progress curve the enzyme activity (U/ml) was calculated.

The HPLC-based assay[57] was used to investigate the behavior of the proteins in presence of variable concentration of magnesium. Reaction mixtures containing HEPES/KOH 27 mM pH 7.5, ATP 1 mM, NMN 1 mM, DTT 1 mM, variable $MgCl_2$ concentrations (0, 20, 50, 100, 500, 2000, 20000 μM), and $H_2O$ to a final volume of 100 μL were incubated in a water bath at 37°C for 10 min. To stop reactions, 50 μL ice-cold 1.2 M $HClO_4$ were added to the single mixtures. After 10 min on ice, the samples were centrifuged 2 min at 16,000*g* and 140 μL aliquot of the perchloric acid supernatants were neutralized by the addition of 27 μL 1 M $K_2CO_3$. The neutralized reactions were frozen at −20°C, thawed, centrifuged 2 min at 16,000*g* and the supernatants were loaded on a 250 × 4.6 mm Supelcosil LC-18T 5 μm reversed-phase HPLC column (Supelco).[57] The amount of NAD was determined from the peak area of the HPLC-separated compounds, with reference to NAD standard, and for each protein the activity was reported as percentage with respect to the activity measured at 20 mM $MgCl_2$.

### *Gel filtration*

The oligomeric state of NMNAT2 mutants was determined by gel filtration on a Superose 12 HR 10/30 column (Pharmacia).[19] A buffer containing 50 mM HEPES, 0.3 M NaCl, and 3 mM DTT was used for elution.

Standard proteins were: BSA (66 kDa), ovalbumin (45 kDa), and carbonic anhydrase (30 kDa). Selected fractions obtained at a flow rate of 0.5 mL/min were analyzed by SDS–PAGE and tested for their NMNAT activity by using the spectrophotometric assay.


## Acknowledgment

We are grateful to Dr. Lucia Cialabrini for her contribution in wt NMNAT2 cloning.


## References


1. Imai S, Armstrong CM, Kaeberlein M, Guarente L (2000) Transcriptional silencing and longevity protein Sir2 is an NAD-dependent histone deacetylase. Nature 403:795–800.
2. North BJ, Marshall BL, Borra MT, Denu JM, Verdin E (2003) The human Sir2 ortholog, SIRT2, is an NAD+-dependent tubulin deacetylase. Mol Cell 11:437–444.
3. Vaziri H, Dessain SK, Ng Eaton E, Imai SI, Frye RA, Pandita TK, Guarente L, Weinberg RA (2001) hSIR2(SIRT1) Functions as an NAD-dependent p53 deacetylase. Cell 107:149–159.
4. Ueda K, Hayaishi O (1985) ADP-ribosylation. Annu Rev Biochem 54:73–100.

5. Bouchard VJ, Rouleau M, Poirier GG (2003) PARP-1, a determinant of cell survival in response to DNA damage. Exp Hematol 31:446–454.
6. Ishizuka S, Martin K, Booth C, Potten CS, de Murcia G, Burkle A, Kirkwood TB (2003) Poly(ADP-ribose) polymerase-1 is a survival factor for radiation-exposed intestinal epithelial stem cells in vivo. Nucleic Acids Res 31:6198–6205.
7. Smith S, Giriat I, Schmitt A, de Lange T (1998) Tankyrase, a poly(ADP-ribose) polymerase at human telomeres. Science 282:1484–1487.
8. Clapper DL, Walseth TF, Dargie PJ, Lee HC (1987) Pyridine nucleotide metabolites stimulate calcium release from sea urchin egg microsomes desensitized to inositol trisphosphate. J Biol Chem 262:9561–9568.
9. Magni G, Amici A, Emanuelli M, Orsomando G, Raffaelli N, Ruggieri S (2004) Structure and function of nicotinamide mononucleotide adenylyltransferase. Curr Med Chem 11:873–885.
10. Magni G, Amici A, Emanuelli M, Raffaelli N, Ruggieri S (1999) Enzymology of NAD+ synthesis. Adv Enzymol Relat Areas Mol Biol 73:135–182, xi.
11. Magni G, Amici A, Emanuelli M, Orsomando G, Raffaelli N, Ruggieri S (2004) Enzymology of NAD+ homeostasis in man. Cell Mol Life Sci 61:19–34.
12. Lau C, Niere M, Ziegler M (2009) The NMN/NaMN adenylyltransferase (NMNAT) protein family. Front Biosci 14:410–431.
13. Zhai RG, Rizzi M, Garavaglia S (2009) Nicotinamide/nicotinic acid mononucleotide adenylyltransferase, new insights into an ancient enzyme. Cell Mol Life Sci 66: 2805–2818.
14. Magni G, Orsomando G, Raffelli N, Ruggieri S (2008) Enzymology of mammalian NAD metabolism in health and disease. Front Biosci 13:6135–6154.
15. Berger F, Lau C, Dahlmann M, Ziegler M (2005) Subcellular compartmentation and differential catalytic properties of the three human nicotinamide mononucleotide adenylyltransferase isoforms. J Biol Chem 280: 36334–36341.
16. Garavaglia S, D'Angelo I, Emanuelli M, Carnevali F, Pierella F, Magni G, Rizzi M (2002) Structure of human NMN adenylyltransferase. A key nuclear enzyme for NAD homeostasis. J Biol Chem 277:8524–8530.
17. Zhou T, Kurnasov O, Tomchick DR, Binns DD, Grishin NV, Marquez VE, Osterman AL, Zhang H (2002) Structure of human nicotinamide/nicotinic acid mononucleotide adenylyltransferase. Basis for the dual substrate specificity and activation of the oncolytic agent tiazofurin. J Biol Chem 277:13148–13154.
18. Werner E, Ziegler M, Lerner F, Schweiger M, Heinemann U (2002) Crystal structure of human nicotinamide mononucleotide adenylyltransferase in complex with NMN. FEBS Lett 516:239–244.
19. Raffaelli N, Sorci L, Amici A, Emanuelli M, Mazzola F, Magni G (2002) Identification of a novel human nicotinamide mononucleotide adenylyltransferase. Biochem Biophys Res Commun 297:835–840.
20. Yalowitz JA, Xiao S, Biju MP, Antony AC, Cummings OW, Deeg MA, Jayaram HN (2004) Characterization of human brain nicotinamide 5'-mononucleotide adenylyltransferase-2 and expression in human pancreas. Biochem J 377:317–326.
21. Di Stefano M, Galassi L, Magni G (2010) Unique expression pattern of human nicotinamide mononucleotide adenylyltransferase isozymes in red blood cells. Blood Cells Mol Dis 45:33–39.
22. Zhang X, Kurnasov OV, Karthikeyan S, Grishin NV, Osterman AL, Zhang H (2003) Structural characterization of a human cytosolic NMN/NaMN adenylyltransferase and implication in human NAD biosynthesis. J Biol Chem 278:13503–13511.
23. Emanuelli M, Carnevali F, Saccucci F, Pierella F, Amici A, Raffaelli N, Magni G (2001) Molecular cloning, chromosomal localization, tissue mRNA levels, bacterial expression, and enzymatic properties of human NMN adenylyltransferase. J Biol Chem 276:406–412.
24. Cooney DA, Jayaram HN, Gebeyehu G, Betts CR, Kelley JA, Marquez VE, Johns DG (1982) The conversion of 2-beta-D-ribofuranosylthiazole-4-carboxamide to an analogue of NAD with potent IMP dehydrogenase-inhibitory properties. Biochem Pharmacol 31:2133–2136.
25. Jager W, Salamon A, Szekeres T (2002) Metabolism of the novel IMP dehydrogenase inhibitor benzamide riboside. Curr Med Chem 9:781–786.
26. Conforti L, Tarlton A, Mack TG, Mi W, Buckmaster EA, Wagner D, Perry VH, Coleman MP (2000) A Ufd2/D4Cole1e chimeric protein and overexpression of Rbp7 in the slow Wallerian degeneration (WldS) mouse. Proc Natl Acad Sci USA 97:11377–11382.
27. Fernando FS, Conforti L, Tosi S, Smith AD, Coleman MP (2002) Human homologue of a gene mutated in the slow Wallerian degeneration (C57BL/Wld(s)) mouse. Gene 284:23–29.
28. Mack TG, Reiner M, Beirowski B, Mi W, Emanuelli M, Wagner D, Thomson D, Gillingwater T, Court F, Conforti L, Fernando FS, Tarlton A, Andressen C, Addicks K, Magni G, Ribchester RR, Perry VH, Coleman MP (2001) Wallerian degeneration of injured axons and synapses is delayed by a Ube4b/Nmnat chimeric gene. Nat Neurosci 4:1199–1206.
29. Gilley J, Coleman MP (2010) Endogenous Nmnat2 is an essential survival factor for maintenance of healthy axons. PLoS Biol 8:e1000300.
30. Yan T, Feng Y, Zheng J, Ge X, Zhang Y, Wu D, Zhao J, Zhai Q (2010) Nmnat2 delays axon degeneration in superior cervical ganglia dependent on its NAD synthesis activity. Neurochem Int 56:101–106.
31. Sorci L, Pan Y, Eyobo Y, Rodionova I, Huang N, Kurnasov O, Zhong S, MacKerell AD, Jr., Zhang H, Osterman AL (2009) Targeting NAD biosynthesis in bacterial pathogens: Structure-based development of inhibitors of nicotinate mononucleotide adenylyltransferase NadD. Chem Biol 16:849–861.
32. Magni G, Di Stefano M, Orsomando G, Raffaelli N, Ruggieri S (2009) NAD(P) biosynthesis enzymes as potential targets for selective drug design. Curr Med Chem 16:1372–1390.
33. Laskowski RA, MacArthur MW, Moss DS, Thornton JM (1993) PROCHECK: a program to check the stereochemical quality of protein structures. J Appl Cryst 26: 283–291.
34. Guex N, Peitsch MC (1997) SWISS-MODEL and the Swiss-PdbViewer: an environment for comparative protein modeling. Electrophoresis 18:2714–2723.
35. Goodsell DS, Morris GM, Olson AJ (1996) Automated docking of flexible ligands: applications of AutoDock. J Mol Recognit 9:1–5.
36. Robertson JG (2005) Mechanistic basis of enzyme-targeted drugs. Biochemistry 44:5561–5571.
37. Rao ST, Rossmann MG (1973) Comparison of super-secondary structures in proteins. J Mol Biol 76:241–256.
38. Linding R, Jensen LJ, Diella F, Bork P, Gibson TJ, Russell RB (2003) Protein disorder prediction: implications for structural proteomics. Structure 11:1453–1459.
39. Schweiger M, Hennig K, Lerner F, Niere M, Hirsch-Kauffmann M, Specht T, Weise C, Oei SL, Ziegler M (2001) Characterization of recombinant human

nicotinamide mononucleotide adenylyl transferase (NMNAT), a nuclear enzyme essential for NAD synthesis. FEBS Lett 492:95–100.
40. Berger F, Lau C, Ziegler M (2007) Regulation of poly (ADP-ribose) polymerase 1 activity by the phosphorylation state of the nuclear NAD biosynthetic enzyme NMN adenylyl transferase 1. Proc Natl Acad Sci USA 104:3765–3770.
41. Carugo O, Cemazar M, Zahariev S, Hudaky I, Gaspari Z, Perczel A, Pongor S (2003) Vicinal disulfide turns. Protein Eng 16:637–639.
42. Emanuelsson O, Brunak S, von Heijne G, Nielsen H (2007) Locating proteins in the cell using TargetP, SignalP and related tools. Nat Protoc 2:953–971.
43. Sorci L, Cimadamore F, Scotti S, Petrelli R, Cappellacci L, Franchetti P, Orsomando G, Magni G (2007) Initial-rate kinetics of human NMN-adenylyltransferases: substrate and metal ion specificity, inhibition by products and multisubstrate analogues, and isozyme contributions to NAD+ biosynthesis. Biochemistry 46:4912–4922.
44. Guex N, Diemand A, Peitsch MC (1999) Protein modelling for all. Trends Biochem Sci 24:364–367.
45. Schwede T, Diemand A, Guex N, Peitsch MC (2000) Protein structure computing in the genomic era. Res Microbiol 151:107–112.
46. Thompson JD, Higgins DG, Gibson TJ (1994) CLUSTAL W: improving the sensitivity of progressive multiple sequence alignment through sequence weighting, position-specific gap penalties and weight matrix choice. Nucleic Acids Res 22:4673–4680.
47. Higgins DG, Thompson JD, Gibson TJ (1996) Using CLUSTAL for multiple sequence alignments. Methods Enzymol 266:383–402.
48. Thompson JD, Gibson TJ, Plewniak F, Jeanmougin F, Higgins DG (1997) The CLUSTAL_X windows interface: flexible strategies for multiple sequence alignment aided by quality analysis tools. Nucleic Acids Res 25:4876–4882.
49. van der Spoel D, Lindahl E, Hess B, Groenhof G, Mark AE, Berendsen HJ (2005) GROMACS: fast, flexible, and free. J Comput Chem 26:1701–1718.
50. Berendsen HJC, van der Spoel D, van Drunen R (1995) GROMACS: a message-passing parallel molecular dynamics implementation. Comp Phys Comm 91:43–56.
51. Berendsen HJC, Postma JPM, van-Gunsteren WF, Hermans J, Interaction models for water in relation to protein hydration. In: Pullman B, Ed. (1981) Intramolecular forces. Dordrecht: D. Reidel Publishing Company, pp 331–342.
52. Darden T, York D, Pedersen L (1993) Particle mesh Ewald: an N-log(N) method for Ewald sums in large systems. J Chem Phys 98:10089–10092.
53. Essmmann U, Perera L, Bertowitz ML, Darden T, Lee H, Pedersen L (1995) A smooth particle mesh Ewald method. J Chem Phys 103:8577–8592.
54. Humphrey W, Dalke A, Schulten K (1996) VMD: visual molecular dynamics. J Mol Graph 14:33–38, 27–38.
55. Schagger H, von Jagow G (1987) Tricine-sodium dodecyl sulfate-polyacrylamide gel electrophoresis for the separation of proteins in the range from 1 to 100 kDa. Anal Biochem 166:368–379.
56. Bradford MM (1976) A rapid and sensitive method for the quantitation of microgram quantities of protein utilizing the principle of protein-dye binding. Anal Biochem 72:248–254.
57. Balducci E, Emanuelli M, Raffaelli N, Ruggieri S, Amici A, Magni G, Orsomando G, Polzonetti V, Natalini P (1995) Assay methods for nicotinamide mononucleotide adenylyltransferase of wide applicability. Anal Biochem 228:64–68.